TẠP CHÍ KHOA HỌC ĐẠI HỌC TÂN TRÀO
ISSN: 2354 - 1431
http://tckh.daihoctantrao.edu.vn/

Anharmonic Correlated Einstein Model and Some Applications to Studies of Thermodynamic Properties and Structural Determination of substances

Nguyen Van Hung[a*]

[a] *Hanoi University of Science*
[*] *Email: hungnv@vnu.edu.vn*

Article info

Recieved:
19/4/2018
Accepted:
12/6/2018

Keywords:
Debye-Waller factor, cumulant expansion, XAFS, thermodynamic properties.

Abstract

This paper presents the anharmonic correlated Einstein model (ACEM) for studying Debye-Waller factors presented in terms of cumulant expansion and some of its applications. The model is derived based on the quantum statistical theory. In addition, the complicated many-particle problem is simplified by the derived anharmonic interatomic effective potential. This includes the many-body effects by the first shell near neighbor contributions to the vibrations between absorber and backscatterer atoms and by projecting these contributions along bond direction to recover the one-dimensional model. Morse potential is assumed to describe the single-pair atomic interaction. Numerical results for several applications are found to be in good agreement with experiment which show the evident temperature dependence of the thermodynamic properties, anharmonic effects and structural parameters of the considered material.

1. Introduction

X-ray Absorption Fine Structure (XAFS) has developed into a powerful technique for providing information on the local atomic structure and thermal effects of substances. The formalism for including anharmonic effects in XAFS is often based on cumulant expansion approach (CEA) [1] from which the anharmonic XAFS function has resulted as [2]

$$\chi(k) = F(k)\frac{e^{-2R/\lambda(k)}}{kR^2}\mathrm{Im}\left\{e^{i\Phi(k)}\exp\left[2ikR+\sum_n\frac{(2ik)^n}{n!}\sigma^{(n)}\right]\right\} \quad (1)$$

where F(k) is the real atomic backscattering amplitude, k and λ are the wave number and mean free path of photoelectron, respectively, Φ is the net phase shift, $R=\langle r\rangle$ with r being the instantaneous bond length between absorber and backscatterer atoms, and $\sigma^{(n)}$ (n = 1, 2, 3, …) are the cumulants describing Debye-Waller factors (DWFs).

Hence, the cumulants or DWFs are very important for the anharmonic XAFS where the even cumulants contribute to the amplitude, the odd ones to the phase of XAFS spectra, and for small anharmonicities, it is sufficient to keep the third and fourth cumulant terms [3]. They are crucial to quantitative treatment of XAFS spectra. Consequently, the lack of the precise DWFs or cumulants has been one of the biggest limitations to accurate structural determinations (e.g., the coordination numbers and the atomic distances) and to specify the other properties of substances from XAFS experiments. Therefore, investigation of DWFs or cumulants and XAFS is of great interest.

Many efforts have been made to overcome such limitations by the theoretical and experimental investigations. The single-bond (SB) correlated Einstein model [4] and single-pair (SP) correlated Debye model [5] have been derived using the CEA to describe the anharmonic effects in XAFS. Unfortunately, they can not provide good agreement of numerical results with

experiment due to neglecting the many-body effects in XAFS of the considered materials.

The purpose of this work is to present the anharmonic correlated Einstein model (ACEM) [6] which can overcome the limitations of SB and SP models and provide good agreement of the numerical results of DWFs presented in terms of cumulant expansion up to the third order and thermal expansion coefficient with experiment, as well as some of its applications to materials studies using XAFS procedures.

2. Anharmonic correlated Einstein model [6]

2.1. Anharmonic interatomic effective potential

In order to include anharmonic effects, the Hamiltonian of system in the present theory for hcp crystals (Zn) involves the anharmonic interatomic effective potential expanded up to the third order as

$$V_{eff}(x) \approx \frac{1}{2}k_{eff}x^2 + k_{3eff}x^3,\ x = r - r_0, \quad (2.1)$$

where k_{eff} is the effective local force constant and k_{3eff} is the cubic anharmonic parameter giving an asymmetry of the anharmonic effective potential, r and r_0 are the instantaneous and equilibrium distances between absorber and backscatterer atoms, respectively.

Determination of parameters k_{eff} and k_{3eff} has been performed based on an Einstein potential [6] or an anharmonic interatomic effective potential derived from the oscillation of a single pair of atoms with masses M_1 and M_2 (e.g., absorber and backscatterer) in a given system. Their oscillation is influenced by their near neighbors. In the center-of-mass frame of this bond it is given by

$$V_{eff}(x) = V(x) + \sum_{i=1,2}\sum_{j\neq i} V\left(\frac{\mu}{M_i}x\hat{\mathbf{R}}_{12}\cdot\hat{\mathbf{R}}_{ij}\right), \quad (2.2)$$

$$\mu = \frac{M_1M_2}{M_1+M_2}$$

where μ is reduced mass of absorber and backscatterer atoms, and $\hat{\mathbf{R}}$ is unit vector; the sum i is over absorber (i = 1) and backscatterer (i = 2), and the sum j is over all their near neighbors, excluding the absorber and backscatterer themselves, whose contributions are described by the term $V(x)$.

Hence, the anharmonic interatomic effective potential given by Eq. (2.2) is quite different from the SP [4] and SB [5] model potentials because it includes not only the term V(x) describing the SP and SB interaction but also the second one describing an affect of lattice on the oscillation between absorber and backscatterer atoms, i.e., the many-body effects have been taken into account. Moreover, by projecting the contributions of the near neighbors of absorber and backscatter along the bond direction as in Eq. (2.2) the one-dimensional model has been recovered that simplifies the many-body problem in XAFS theory.

In the ACEM the Morse potential expanded to the third order around its minimum

$$V(x) = D\left(e^{-2\alpha x} - 2e^{-\alpha x}\right) \approx D\left(-1 + \alpha^2x^2 - \alpha^3x^3 + \cdots\right), \quad (2.3)$$

is assumed to describe the single-pair atomic interaction included in the anharmonic effective potential where 1/α describes the width of the potential and D is the dissociation energy. It is usually sufficient to consider weak anharmonicity (i.e., first-order perturbation theory) so that only the cubic term in this equation must be kept.

For deriving XAFS cumulants we describe the anharmonic interatomic effective potential given by Eq. (2) in the summation of the harmonic contribution and a perturbation δV due to the weak anharmonicity as

$$V_{eff}(y) = \frac{1}{2}k_{eff}y^2 + \delta V(y),$$

$$\delta V \cong 5D\alpha^2 ay + k_{3eff}y^3,\ y = x - a,\ a = \langle x\rangle. \quad (2.4)$$

2.2. XAFS cumulants and thermal expansion coefficient

The derivation of XAFS cumulants in ACEM is based on quantum statistical theory [7] and the parameters of the anharmonic interatomic effective potentials given by Eqs. (2.2) and (2.4), as well as an averaging procedure using the canonical partition function Z and statistical density matrix ρ, e.g.,

$$\langle y^m\rangle = \frac{1}{Z}Tr\left(\rho y^m\right),\quad m = 1, 2, 3, \cdots \quad (2.5)$$

Atomic vibrations are quantized in terms of phonons, and anharmonicity is the result of phonon-phonon interaction, that is why we express y in terms of the

annihilation and creation operators, $\hat{a}$ and $\hat{a}^+$, respectively

$$y \equiv a_0\left(\hat{a}+\hat{a}^+\right), \quad a_0 = \sqrt{\frac{\hbar\omega_E}{10D\alpha^2}}, \qquad (2.6)$$

which have the following properties

$$\begin{aligned} &\left[\hat{a},\hat{a}^+\right]=1,\ \hat{a}^+\left|n\right\rangle=\sqrt{n+1}\left|n+1\right\rangle, \\ &\hat{a}\left|n\right\rangle=\sqrt{n-1}\left|n-1\right\rangle,\ \hat{a}^+\hat{a}\left|n\right\rangle=n\left|n\right\rangle \end{aligned}, \qquad (2.7)$$

as well as use the harmonic oscillator state $\left|n\right\rangle$ as the eigenstate with the eigenvalue $E_n = n\hbar\omega_E$ for n being the phonon number, ignoring the zero-point energy for convenience.

Due to weak anharmonicity in XAFS, the canonical partition function in Eq. (2.5) can be expressed as

$$\begin{aligned} &Z \cong Z_0 = \sum_n e^{-n\beta\hbar\omega_E} = \sum_{n=0}^{\infty} z^n = \frac{1}{1-z}, \\ &z = \exp\left(-\theta_E / T\right) \end{aligned}, \qquad (2.8)$$

where the correlated Einstein frequency ω_E and temperature θ_E of hcp crystals are given by

$$\omega_E = \sqrt{\frac{10D\alpha^2}{M}}, \qquad \theta_E = \frac{\hbar\omega_E}{k_B}, \qquad (2.9)$$

M is the atomic mass and k_B is Boltzmann constant.

Using the above results for the correlated atomic vibration and the procedure depicted by Eqs. (2.5) - (2.9), as well as the first-order thermodynamic perturbation theory [7], the temperature-dependent XAFS cumulants have been derived.

Based on the procedure depicted by Eq. (2.5) we derived the even moment expressing the second cumulant or MSRD

$$\begin{aligned} &\sigma^2(T) = \left\langle y^2 \right\rangle = \sum_n e^{-n\beta\hbar\omega_E} \left\langle n\left| y^2 \right| n\right\rangle, \\ &\beta = 1/k_B T \end{aligned}, \qquad (2.10)$$

and the odd moments expressing the first (m = 1) and third (m = 3) cumulants

$$\begin{aligned} &\left\langle y^m \right\rangle = \frac{k_{eff}}{Z_0} \sum_{n,n'} \frac{e^{-\beta E_n} - e^{-\beta E_{n'}}}{E_n - E_{n'}} \left\langle n\left|\delta V(y)\right| n'\right\rangle \left\langle n'\left| y^m \right| n\right\rangle, \\ &m = 1,3 \end{aligned}, \qquad (2.11)$$

where the operations expressed by Eqs. (2.5) and (2.6) have been applied to calculate the matrix elements given in Eqs. (2.10) and (2.11).

Consequently, the XAFS expressions have resulted for the second cumulant or MSRD

$$\sigma^2(T) = \left\langle y^2 \right\rangle = \sigma_0^2 \frac{1+z(T)}{1-z(T)},\ \sigma_0^2 = \frac{\hbar\omega_E}{10D\alpha^2}, \qquad (2.12)$$

for the first cumulant or net thermal expansion

$$\begin{aligned} &\sigma^{(1)}(T) = a = \sigma_0^{(1)} \frac{1+z(T)}{1-z(T)} = \frac{\sigma_0^{(1)}}{\sigma_0^2}\sigma^2(T), \\ &\sigma_0^{(1)} = \frac{3\alpha}{4}\sigma_0^2 \end{aligned}, \qquad (2.13)$$

and for the third cumulant or mean cubic relative displacement (MCRD)

$$\begin{aligned} &\sigma^{(3)}(T) = \left\langle y^3 \right\rangle = \sigma_0^{(3)} \frac{3\left(\sigma^2\right)^2 - 2\left(\sigma_0^2\right)^2}{\left(\sigma_0^2\right)^2}, \\ &\sigma_0^{(3)} = \frac{\alpha}{2}\left(\sigma_0^2\right)^2 \end{aligned}, \qquad (2.14)$$

Moreover, using the first cumulant given by Eq. (2.13), the expression for the thermal expansion coefficient has been derived and given by

$$\begin{aligned} &\alpha_T(T) = \frac{1}{r}\frac{da}{dT} = \alpha_T^0 \left(\frac{5D\alpha^2}{k_B T}\right)^2 \left[1 - \left(\sigma_0^2/\sigma^2\right)^2\right], \\ &\alpha_T^0 = \frac{3k_B}{20D\alpha r} \end{aligned}, \qquad (2.15)$$

From the above results a simple relation between cumulants in term of σ^2 has resulted as

$$\frac{\sigma^{(1)}\sigma^2}{\sigma^{(3)}} = \frac{1}{2-(4/3)(\sigma_0^2/\sigma^2)^2}, \qquad (2.16)$$

which approaches the classical expression [8] of 1/2 at high temperatures.

In the above expressions the temperature variable has been described in terms of σ^2 as

$$z = \frac{\sigma^2 - \sigma_0^2}{\sigma^2 - \sigma_0^2}, \qquad (2.17)$$

$\sigma_0^{(1)}$, σ_0^2, $\sigma_0^{(3)}$ are zero-point energy contributions to three first XAFS cumulants $\sigma^{(1)}(T)$, $\sigma^2(T)$, $\sigma^{(3)}(T)$, respectively, and α_T^0 is the constant value which the thermal expansion coefficient approaches at high-temperatures.

The above formulas at low and high temperatures are presented in Table 2.1.

Table 2.1. *Formulas of $\sigma^{(1)}$, σ^2, $\sigma^{(3)}$, and α_T in low temperature ($T \to 0$) and high temperature ($T \to \infty$) limits.*

	T→0	T→∞
$\sigma^{(1)}$	$\sigma_0^{(1)}(1+2z)$	$(3k_B/20D\alpha)T$
σ^2	$\sigma_0^2(1+2z)$	$(k_B/5D\alpha^2)T$
$\sigma^{(3)}$	$\sigma_0^{(3)}(1+12z)$	$(3k_B^2/50D^2\alpha^3)T^2$
α_T	$\alpha_T^0 z(\ln z)^2(1+2z)$	α_T^0

Hence, the first and second cumulants are linearly proportional to the temperature T, the third cumulant to T^2, and the thermal expansion coefficient α_T approaches the constant value α_T^0 at high temperatures, while the cumulants contain zero-point energy contributions, a quantum effect, and α_T vanishes exponentially at low temperatures.

2.3. Numerical results and discussions

Now the expressions derived in the previous section are applied to numerical calculations for XAFS cumulants and thermal expansion coefficient of Cu using its Morse potential parameters [9] D = 0.343 eV and α = 1.359 $Å^{-1}$. Anharmonic effective potential of Cu is presented in Fig. 2.1 which is asymmetric compared to the harmonic term due to anharmonic contribution.

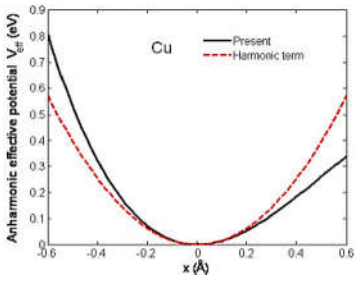

Fig. 2.1. *Anharmonic interatomic effective potential of Cu calculated using the present theory and its Morse parameters [9].*

Fig. 2.2 illustrates good agreement of temperature dependence of (a) first cumulant $\sigma^{(1)}$(T) and (b) second cumulant σ^2(T) of Cu calculated using the present theory with the experimental values of Beccara et al [10] for the first cumulant and of Greegor et al [11] and Yokoyama et al [12] for the second cumulant. Here, the value of σ^2(295 K) of SP potential [5] is also presented for comparison. Here, $\sigma^{(1)}$(T) and σ^2(T) are linearly proportional to the temperature at high temperatures and contain zero-point energy contribution at low temperatures, a quantum effect.

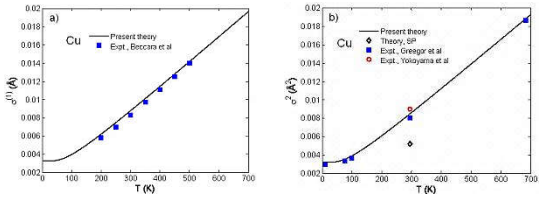

Fig. 2.2. *Temperature dependence of (a) first cumulant $\sigma^{(1)}$(T) and (b) second cumulant σ^2(T) of Cu calculated using the present theory compared to the experimental values of Beccra et al [10] for the first cumulant, of Greegor et al [11] and Yokoyama et al [12] for the second cumulant. Here, the value of σ^2(295 K) of SP potential [5] is also presented for comparison.*

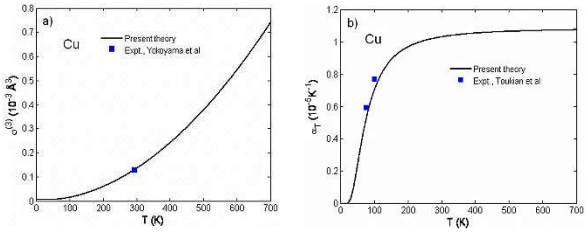

Fig. 2.3. *Temperature dependence of (a) third cumulant $\sigma^{(3)}$(T) and (b) thermal expansion coefficient α_T (T) of Cu calculated using the present theory compared to the experimental values of Yokoyama et al [12] for the third cumulant and of Toukian et al [13] for the thermal expansion coefficient.*

Table 2.2. *Comparison of second, third cumulants and thermal expansion coefficient of Cu calculated using the present theory compared to experiment and to those of other theory.*

	σ^2 ($\times 10^{-2}$ Å^2)			$\sigma^{(3)}$ ($\times 10^{-3}$ Å^3)		α_T ($\times 10^{-5}$ K^{-1})	
T (K)	Present	Expt.[a]	Other[b]	Present	Expt.[c]	Present	Expt.[d]
10	0.298	0.292					
77	0.333	0.325		0.010		0.584	0.59
100	0.365			0.014		0.745	0.80
295	0.803	0.774	0.520	0.131	0.13	1.070	
300	0.817			0.136		1.072	
683	1.858	1.823				1.090	

[a]Ref. 11, [b]Ref. 5, [c]Ref. 12, [d]Ref. 13.

The good agreement of temperature dependence of third cumulant $\sigma^{(3)}$(T) of Cu calculated using the present theory with the experimental values of Yokoyama et al [12] is presented in Fig. 2.3a. Such good agreement of the calculated thermal expansion coefficient α_T (T) of Cu with the experimental values of Toukian et al [13] is shown in Fig. 2.3b. Here, the third cumulant is proportional to square of temperature

and α_T approaches the constant value at high temperatures.

Comparison of second, third cumulants and thermal expansion coefficient of Cu calculated using the present theory with the experimental values [11-13] and with those of other theory [5] is presented in Tab. 2.2.

3. Classical ACEM [14]

3.1. High-order expanded Debye-Waller factor in classical ACEM

Classical theory has the advantage of applications up to high-temperatures, even up to melting temperatures [8]. Within the classical limit and the assumption that the anharmonicity can be treated as a small perturbation, the temperature-dependent moments with using the anharmonic effective potentials given by Eq. (2.2), about the mean <*x*>, as determined by evaluating the thermal average

$$\left\langle (x-\langle x\rangle)^n \right\rangle = \frac{\int_{-\infty}^{\infty}(x-\langle x\rangle)^n \exp\left[-\frac{V_{eff}(x)}{k_BT}\right]dx}{\int_{-\infty}^{\infty}\exp\left[-\frac{V_{eff}(x)}{k_BT}\right]dx} \quad (3.1)$$

$$\cong \frac{\int_{-\infty}^{\infty}(x-\langle x\rangle)^n \exp\left[-\frac{k_{eff}x^2}{2k_BT}\right]\left[\sum_{n=0}^{3}\frac{1}{n!}\left(\frac{k_{3eff}x^3-k_{4eff}x^4}{k_BT}\right)^n\right]dx}{\left(\frac{2\pi k_BT}{k_{eff}}\right)^{1/2}\left[1+\frac{3(k_BT)}{k_{eff}^2}\left(\frac{5k_{3eff}^2}{2k_{eff}}-k_{4eff}\right)\right]}$$

to the lowest orders in T are given by

$$\langle x\rangle = \frac{3k_BT}{20D\alpha}\left[1+\frac{k_BT}{25D\alpha}\left(\frac{133}{6}\alpha+45\right)\right], \quad (3.2)$$

$$\left\langle (x-\langle x\rangle)^2 \right\rangle = \frac{k_BT}{5D\alpha^2}\left[1+\frac{3k_BT}{5D\alpha^3}\left(\frac{133}{48}\alpha^3+\frac{15}{4}\right)\right], \quad (3.3)$$

$$\left\langle (x-\langle x\rangle)^3 \right\rangle = \frac{3(k_BT)^2}{50D^2\alpha^3}\left(1+\frac{2637}{800}\frac{k_BT}{D}\right), \quad (3.4)$$

$$\left\langle (x-\langle x\rangle)^4 \right\rangle = \frac{3(k_BT)^2}{25D^2\alpha^4}\left(1+\frac{139}{300}\frac{k_BT}{D}\right), \quad (3.5)$$

where the effective parameters k_{eff}, k_{3eff} and k_{4eff} of the high-order anharmonic effective potential for hcp crystals contained in Eqs. (3.2-9) have been substituted by their values in terms of Morse potential parameters.

The truncation of the series in Eq. (3.1) serves as a convergence cutoff while including enough terms to accurately obtain the second lowest-order expressions for the moments. The respective expressions obtained from Eqs. (3.2- 5) to lowest order in the temperature T are given by for the first cumulant or net thermal expansion

$$\sigma^{(1)} = \left\langle r-r_0 \right\rangle = \left\langle x \right\rangle = \frac{3}{4}\alpha\sigma^2, \quad (3.6)$$

for the second cumulant or MSRD

$$\sigma^2 = \left\langle (r-r_0)^2 \right\rangle \cong \left\langle x^2 \right\rangle = \frac{k_BT}{5D\alpha^2} = \frac{2k_BT}{m\omega_E^2}, \quad (3.7)$$

for the third cumulant

$$\sigma^{(3)} = \left\langle (r-r_0)^3 \right\rangle \cong \left\langle x^3 \right\rangle - 3\sigma^{(1)}\sigma^2 = \frac{3}{2}\alpha\left(\sigma^2\right)^2. \quad (3.8)$$

and for the fourth cumulant

$$\sigma^{(4)} = \left\langle (r-r_0)^4 \right\rangle - 3\left(\sigma^2\right)^2 \cong \left\langle x^4 \right\rangle - 3\left(\sigma^2\right)^2 = \frac{137}{40}\alpha^2\left(\sigma^2\right)^3, \quad (3.9)$$

as well as for the cumulant ratio

$$\frac{\sigma^{(1)}\sigma^2}{\sigma^{(3)}} = \frac{1}{2}, \quad (3.10)$$

where ω_E is the correlated Einstein frequency.

Hence, thanks to using the derived anharmonic effective potential, all the obtained cumulants given by Eqs. (3.6-9) have been presented in very simple forms in terms of second cumulant or MSRD. It is useful not only for reducing the numerical calculations, but also for obtaining or predicting the other theoretical or experimental XAFS cumulants based on the calculated or measured second cumulant. Since the second cumulant σ^2 given by Eq. (3.2) is proportional to the temperature T, the first cumulant $\sigma^{(1)}$ is also linear with T, and the third and fourth cumulants vary as T^2 and T^3, respectively. Moreover, Eq. (3.2) shows inverse proportionality of this second cumulant σ^2 to the square of correlated Einstein frequency ω_E^2, so that from Eqs. (3.6-9), the cumulants $\sigma^{(1)}$, $\sigma^{(3)}$ and $\sigma^{(4)}$ are inversely proportional to ω_E^2, ω_E^4 and ω_E^6, respectively. The cumulant ratio $\sigma^{(1)}\sigma^2/\sigma^{(3)}$ is often considered as a standard for cumulant study. Its value of 1/2 given by Eq. (3.10) is

valid for all temperatures, while such ratio resulted from quantum theory, approaches 1/2 only at high temperatures [6,15].

3.2. Numerical results for hcp crystals and discussions

For discussing the successes and efficiencies of the developments in this work, the expressions derived in the previous section have been applied to numerical calculations of the anharmonic interatomic effective potentials and four first temperature-dependent XAFS cumulants of Zn and Cd using Morse potential parameters [15] D = 0.1698 eV, α = 1.7054 $Å^{-1}$ for Zn and D = 0.1675 eV, α = 1.9069 $Å^{-1}$ for Cd, as well as their experimental values [16] D = 0.1685 eV, α = 1.700 $Å^{-1}$ for Zn and D = 0.1653 eV, α = 1.9053 $Å^{-1}$ for Cd.

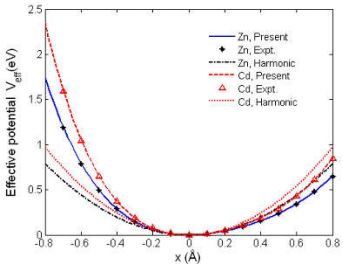

Fig. 3.1. *High-order anharmonic interatomic effective potentials of Zn and Cd calculated using the present theory compared to experiment obtained from the measured Morse potential parameters [16] and to their calculated harmonic terms.*

Fig. 3.1 illustrates good agreement of the anharmonic effective potentials of Zn and Cd expanded up to the fourth order calculated using the present theory with experiment obtained from the measured Morse potential parameters [16]. They are significantly asymmetric compared to their harmonic terms due to including the anharmonic contributions given by k_{3eff} and k_{4eff}. These calculated anharmonic effective potentials are used for the calculation and analysis of four first XAFS cumulants of Zn and Cd.

Temperature dependence of first cumulant or net thermal expansion $\sigma^{(1)}$(T) (Fig. 3.2a) and second cumulant or MSRD σ^2(T) (Fig. 3.2b) of Zn and Cd calculated using the present theory agrees well with the experimental value at 300 K. The limitation here is unsatisfactory of the agreement of the calculated values of $\sigma^{(1)}$(T), σ^2(T) of Zn and Cd with experiment at 77 K. It is an evident limitation of any classical theory including the present one due to the absent of zero-point vibrations. The lowest temperature at which the classical limit can be applied to the first and second cumulants is about the correlated Einstein temperature θ_E = 205.61 K for Zn, and θ_E = 174.14 K for Cd calculated using the present theory.

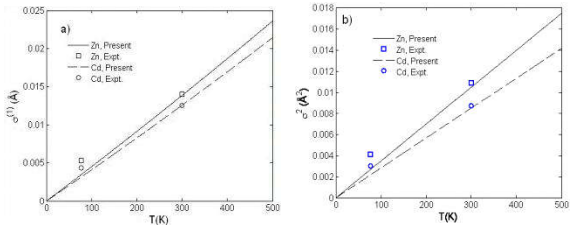

Fig. 3.2. *Temperature dependence of (a) first cumulant $\sigma^{(1)}$(T) and (b) second cumulant σ^2(T) calculated using the present theory for Zn and Cd compared to the experimental values at 77 K and 300 K [16].*

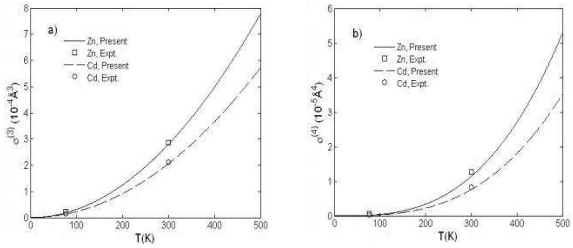

Fig. 3.3. *Temperature dependence of a) third cumulant $\sigma^{(3)}$ (T) and b) fourth cumulant $\sigma^{(4)}$ (T), calculated using the present theory for Zn and Cd compared to the experimental values at 77 K and 300 K [16].*

Unfortunately, this limitation is significantly reduced for the third and fourth cumulants. Temperature dependence of the third cumulant $\sigma^{(3)}(T)$ (Fig. 3.3a) and the fourth cumulant $\sigma^{(4)}$(T) (Fig. 3.3b) for Zn and Cd calculated using the present theory agrees well with experiment not only at 300 K but also at 77 K. Hence, the present classical theory can be applied to the third and fourth cumulants of hcp crystals from the temperatures which are much lower than their Einstein temperatures. The reason of the above conclusions is attributed to the absent of zero-point vibrations, which are non-negligible for the first and second cumulants, and negligibly small for the third and fourth cumulants. Despite such limitation to the first and second cumulants, the present theory is suited for describing anharmonic effects in XAFS using

cumulant expansion, because anharmonicity appears apparently from about room temperature [6].

The cumulant ratio $\sigma^{(1)}\sigma^2/\sigma^{(3)}$ is often considered as a standard for cumulant study [16]. Fig. 3.4 illustrates the equality to 1/2 of $\sigma^{(1)}\sigma^2/\sigma^{(3)}$ for Zn and Cd calculated using the present theory for all temperatures, while this ratio obtained from quantum theory approaches 1/2 only at high temperatures [6].

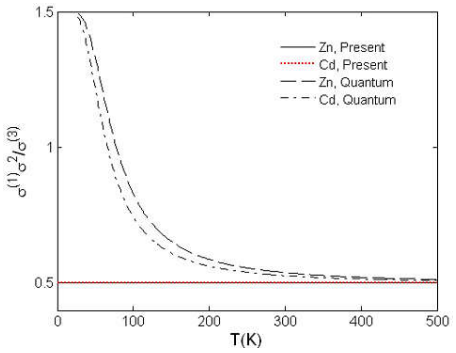

Fig. 3.4. *Temperature dependence of cumulant ratio $\sigma^{(1)}\sigma^2/\sigma^{(3)}$ of Zn and Cd calculated usingthe present theory compared to those obtained from quantum statistical theory [16].*

Note that the experimental values of the first, second, third and fourth cumulants of Zn and Cd at 77 K and 300 K compared to our calculated results presented in the above figures have been extracted from XAFS spectra measured at HASYLAB (DESY, Germany) by a fitting procedure [16]. Moreover, the above numerical results for Zn and Cd have confirmed the proportionality of the first and second cumulants to the temperature T, the third and fourth cumulants to T^2 and T^3, respectively.

4. Application to theoretical and experimental XAFS studies of hcp crystals [17]

4.1. Advanced method for theoretical and experimental XAFS studies of hcp crystals

In this application the ACEM [6] has further developed into an advanced method using that not only theoretical but also experimental XAFS quantities including not only cumulants but also XAFS spectra and their Fourier transform magnitudes can be provided based on only the calculated and measured second cumulants or MSRDs which has the form

$$\sigma^2(T)=\sigma_0^2\frac{1+z(T)}{1-z(T)},\ \sigma_0^2=\frac{\hbar\omega_E}{10D\alpha^2},\qquad (4.1)$$
$$z(T)=\exp\left(\theta_E/T\right)$$

Hence, we have the expressions for the first cumulant or net thermal expansion

$$\sigma^{(1)}(T)=\sigma_0^{(1)}\frac{1+z(T)}{1-z(T)}=\frac{\sigma_0^{(1)}}{\sigma_0^2}\sigma^2(T),\qquad (4.2)$$
$$\sigma_0^{(1)}=\frac{3\alpha}{4}\sigma_0^2$$

for the third cumulant or mean cubic relative displacement (MCRD)

$$\sigma^{(3)}(T)=\sigma_0^{(3)}\left[3\left(\frac{\sigma^2(T)}{\sigma_0^2}\right)^2-2\right],\qquad (4.3)$$
$$\sigma_0^{(3)}=\frac{\alpha}{2}\left(\sigma_0^2\right)^2$$

and for the thermal expansion coefficient

$$\alpha_T(T)=\alpha_T^0\frac{\left(\sigma^2(T)\right)^2-\left(\sigma_0^2\right)^2}{T^2},\qquad (4.4)$$
$$\alpha_T^0=\frac{15D\alpha^3}{4k_Br}$$

Moreover, the second cumulant given by Eq. (4.1) is harmonic while the experimental data always include the temperature-dependent anharmonic effects. That is why we introduce the total second cumulant or MSRD as

$$\sigma_{tot}^2(T)=\sigma^2(T)+\sigma_A^2(T),\qquad (4.5)$$

which involves an anharmonic contribution

$$\sigma_A^2(T)=\beta_A(T)\left[\sigma^2(T)-\sigma_0^2\right],\qquad (4.6)$$

containing the anharmonic factor

$$\beta_A(T)=\frac{9\alpha^2}{8}\sigma^2(T)\left[1+\frac{3\alpha}{4R}\sigma^2(T)\left(1+\frac{3\alpha}{4R}\sigma^2(T)\right)\right],\qquad (4.7)$$

Further, we develop the XAFS function given by Eq. (1) into an analytical form explicitly including the above obtained cumulants for the temperature-dependent K-edge anharmonic XAFS spectra as

$$\chi(k,T)=\sum_j\frac{S_0^2N_j}{kR_j^2}F_j(k)F_A(k,T)e^{-\left(2k^2\sigma^2(T)+2R_j/\lambda(k)\right)}\qquad (4.8)$$
$$\sin\left(2kR_j+\Phi_j(k)+\Phi_A^j(k,T)\right)$$

which contains the anharmonic contribution to amplitude described by an factor

$$F_A(k,T)=\exp\left[-2k^2\sigma_A^2(T)\right],\qquad (4.9)$$

causing the anharmonic attenuation and the anharmonic contribution to phase

$$\Phi_A(T,k) = 2k\left[\sigma^{(1)}(T) - 2\sigma_A^2(T)\left(\frac{1}{R} - \frac{1}{\lambda(k)}\right) - \frac{2}{3}\sigma^{(3)}(T)k^2\right] \quad (4.10)$$

causing the anharmonic phase shift of XAFS spectra.

In the anharmonic XAFS function Eq. (4.8) S_0^2 is the square of the many body overlap term, N_j is the atomic number of each shell, the mean free path λ is defined by the imaginary part of the complex photoelectron momentum $p = k + i/\lambda$, and the sum is over all considered atomic shells. Moreover, all parameters of this function can be obtained from the second cumulant or MSRD, and this function will return to the harmonic case calculated by the well-known FEFF code [18] if the anharmonic contributions to amplitude $F_A(k,T)$ and to phase $\Phi_A(k,T)$ are excluded. Inversely, the FEFF code can also be modified by including these anharmonic contributions to XAFS amplitude and phase to calculate the anharmonic XAFS spectra and their Fourier transform magnitudes. It is the evident advantage of the present method which will be applied to the numerical calculations and to the extractions of experimental XAFS parameters for Zn presented in Section 4.2.

4.2. Experimental and numerical results and discussions

4.2.1. Experimental

The measurements of the second cumulant, XAFS spectra and their Fourier transform magnitudes of Zn at 300 K, 400 K, 500 K and 600 K have been performed at the Beamline BL8, SLRI (Thailand). It is the routinely operated for X-ray absorption spectroscopy (XAS) in an immediate photon energy range (1.25 - 10 keV). The experimental set-up conveniently facilitates XAS measurements in transmission and fluorescence-yield modes at several K-edges of elements ranging from Magnesium to Zinc [19]. The experimental values of the first, third cumulants, thermal expansion coefficients and some other XAFS parameters of Zn at 300 K, 400 K, 500 K and 600 K have been extracted from the measured values of the second cumulant using the present method based on the description of these quantities in terms of second cumulant presented in Section 4.1. The obtained experimental results will be presented in Section 4.2 compared to the theoretical results.

4.2.2. Numerical calculation results compared to experiment and discussions

Now the expressions derived in the previous Section 2 are applied to numerical calculations for Zn using its Morse potential parameters [15] D = 0.1700 eV, α = 1.7054 Å^{-1} which were obtained using experimental values for the energy of sublimation, the compressibility, and the lattice constant.

4.2.2.1. XAFS cumulants and thermal expansion coefficient

Fig. 4.1 illustrates good agreement of (a) first cumulant $\sigma^{(1)}(T)$ and (b) total and harmonic second cumulants $\sigma_{tot}^2(T)$, $\sigma^2(T)$, respectively, of Zn calculated using the present theory with the experimental values at 300 K, 400 K, 500 K, and 600 K. Here, $\sigma_{tot}^2(T)$ is a little different from $\sigma^2(T)$ at temperatures greater than the room temperature due to the temperature-dependent anharmonic contributions. Note that using this first cumulant we can obtain temperature dependence of the first shell near neighbor distance based on the expression $R(T) = R(0) + \sigma^{(1)}(T)$.

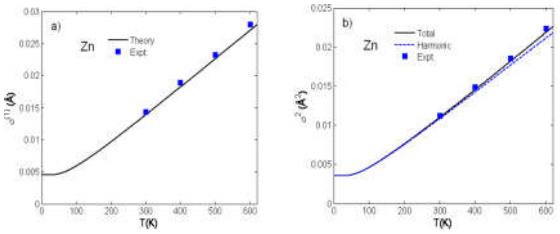

Fig. 4.1. *Temperature dependence of (a) first cumulant $\sigma^{(1)}(T)$ and (b) total and harmonic second cumulants $\sigma_{tot}^2(T)$ and $\sigma^2(T)$, respectively, of Zn calculated using the present theory compared to the experimental values at 300 K, 400 K, 500 K and 600 K.*

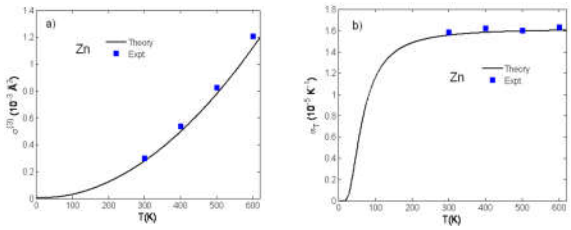

Fig. 4.2. *Temperature dependence of (a) third cumulant $\sigma^{(3)}(T)$ and (b) thermal expansion coefficient $\alpha_T(T)$ of Zn calculated using the present theory*

compared to the experimental values at 300 K, 400 K, 500 K and 600 K.

Temperature dependence of third cumulant $\sigma^{(3)}(T)$ (Fig. 4.2a) and thermal expansion coefficient $\alpha_T(T)$ (Fig. 4.2b) of Zn calculated using the present theory agrees well with the experimental values at 300 K, 400 K, 500 K and 600 K. Here, the theoretical and experimental thermal expansion coefficients of Zn approach the constant values at high-temperatures as it was obtained for the other crystal structures [11, 22-26].

Figs. 4.3 illustrate good agreement of temperature dependence of (a) anharmonic contributions $\sigma_A^2(T)$ to the second cumulant or MSRD and (b) anharmonic factor $\beta_A(T)$ of Zn calculated using the present theory with their experimental values at 300 K, 400 K, 500 K and 600 K where $\beta_A(T)$ characterizes percentage of the anharmonic contributions at each temperature. These values are normally difficult to be directly measured, but using the present method they have been calculated and extracted from the calculated and measured second cumulants.

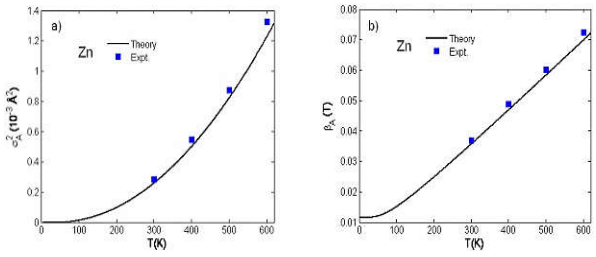

Fig. 4.3. *Temperature dependence of (a) anharmonic contribution $\sigma_A^2(T)$ to second cumulant or MSRD and (b) anharmonic factor $\beta_A(T)$ of Zn calculated using the present theory compared to the experimental values at 300 K, 400 K, 500 K and 600 K.*

The cumulant ratios $\sigma^{(1)}\sigma^2/\sigma^{(3)}$ and $\alpha_T T\sigma^2/\sigma^{(3)}$ are often considered as the standards for cumulant studies [6,16] and to identify the temperature above which the classical limit is applicable [6]. Figs. 4.4 show good agreement of temperature dependence of (a) $\sigma^{(1)}\sigma^2/\sigma^{(3)}$ and (b) $\alpha_T T\sigma^2/\sigma^{(3)}$ of Zn calculated using the present theory with the experimental values at 300 K, 400 K, 500 K and 600 K. The theoretical and experimental results of these ratios show that above the Einstein temperature (θ_E = 206 K calculated using the present theory for Zn) they approach the classical value [8,14] of 1/2 so that the classical limit is applicable.

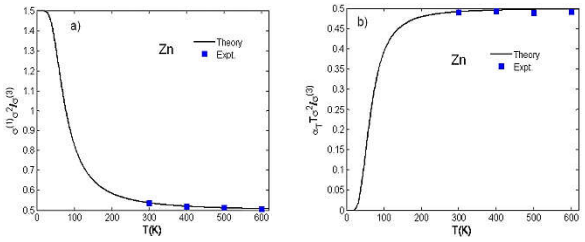

Fig. 4.4. *Temperature dependence of cumulant ratios (a) $\sigma^{(1)}\sigma^2/\sigma^{(3)}$ and (b) $\alpha_T T\sigma^2/\sigma^{(3)}$ of Zn calculated using the present theory compared to the experimental values at 300 K, 400 K, 500 K and 600 K.*

Table 4.1 illustrates good agreement of the values of three first XAFS cumulants and thermal expansion coefficients of Zn calculated using the present theory at 300 K, 400 K, 500 K and 600 K with their experimental values.

Table 4.1. *Comparison of the values of three first XAFS cumulants and thermal expansion coefficients of Zn calculated using the present theory with their experimental values at 300 K, 400 K, 500 K and 600 K.*

T(K)	$\sigma^{(1)}$(Å)	$\sigma^{(1)}$(Å)	σ^2(Å^2)	σ^2(Å^2)	σ^2(Å^2)	$\sigma^{(3)}$(Å^3)	$\sigma^{(3)}$(Å^3)	α_T(10^{-5}/K)	α_T(10^{-5}/K)
	Theory	Expt.	Total	Harm.	Expt.	Theory	Expt.	Theory	Expt.
300	0.0139	0.0143	0.0110	0.0109	0.0113	0.0003	0.0003	1.555	1.582
400	0.0182	0.0189	0.0146	0.0143	0.0149	0.0005	0.0006	1.582	1.618
500	0.0226	0.0232	0.0182	0.0177	0.0185	0.0008	0.0009	1.595	1.599
600	0.0270	0.0279	0.0219	0.0211	0.0223	0.0011	0.0012	1.602	1.630

The second cumulant describing MSRD is primary a harmonic effect plus small anharmonic contributions which appear only at high-temperatures. But the first cumulant describing the net thermal expansion or lattice disorder, the third cumulant or MCRD describing the asymmetry of pair atomic distribution function and the thermal expansion coefficient are entirely anharmonic effects because they appear due to including the cubic anharmonic effective potential parameter.

4.2.2.2. XAFS spectra and their Fourier transform magnitudes

Based on the present advanced method, the FEFF code [18] has been modified by including the amharmonic contributions to XAFS amplitude and phase described by the above obtained cumulants to calculate XAFS spectra at 300 K, 400 K, 500 K, 600

K of Zn and their Fourier transform magnitudes. Figs. 4.5 illustrate the anharmonic (a) attenuation factor $F_A(k,T)$ and (b) phase shift $\Phi_A(k,T)$ of XAFS of Zn at 300 K, 400 K, 500 K, and 600 K calculated using the present theory including the above obtained cumulants. These values increase showing the increase of anharmonicity as k-value and temperature T increase. Using these values of $F_A(k,T)$ and $\Phi_A(k,T)$, the anharmonic XAFS spectra of Zn at 300 K, 400 K, 500 K and 600 K have been calculated and presented in Fig. 4.6a compared to the measured results presented in Fig. 4.6b. The anharmonic amplitude attenuation and phase shift are evidently shown in both theoretical and experimental XAFS spectra. These theoretical and experimental anharmonic XAFS spectra have been Fourier transformed and their Fourier transform magnitudes are presented in Fig. 4.7. They show good agreement between the theoretical and experimental results, as well as the decrease of the peak heights and their shifts to the left as the temperature T increases.

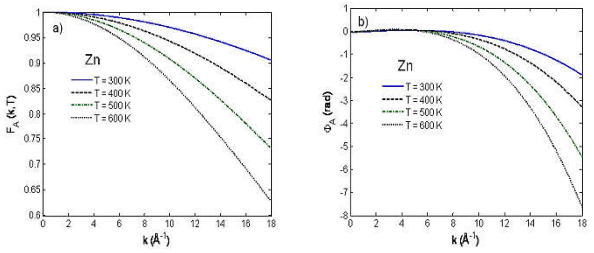

Fig. 4.5. *The wave number k and temperature T dependence of the anharmonic (a) attenuation factor $F_A(k,T)$ and (b) phase shift $\Phi_A(k,T)$ of XAFS of Zn at 300 K, 400 K, 500 K, and 600 K calculated using the present theory.*

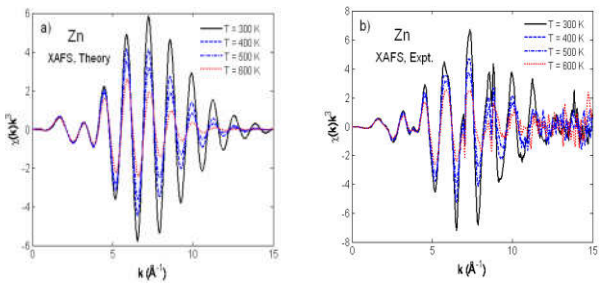

Fig. 4.6. *(a) Theoretical and (b) experimental XAFS spectra of Zn at 300 K, 400 K, 500 K, 600 K.*

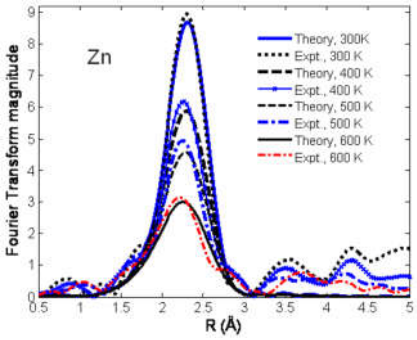

Fig. 4.7. *Comparison of Fourier transform magnitudes of XAFS spectra of Zn at 300 K, 400 K, 500 K, and 600 K calculated using the present theory with their experimental results.*

Note that the anharmonic XAFS spectra of Zn at 300 K, 400 K, 500 K and 600 K and their Fourier transform magnitudes have been calculated based on including the anharmonic contributions to XAFS amplitude and phase using the cumulants obtained from the second cumulants or MSRDs. The results are found to be in good agreement with the measured data. Moreover, using the present theory and the measured second cumulants of Zn at 300 K, 400 K, 500 K, 600 K we have reproduced all the considered experimental values including XAFS spectra and their Fourier transform magnitudes. The obtained results agree well with the experimental values at these temperatures.

Moreover, some international scientists have successfully used the ACEM [20-24] and called it Hung and Rehr theory or Hung and Rehr method. According to ResearchGate we got 150 international citations which mostly focuses on the ACEM.

5. Conclusions

In this paper, the ACEM and some of its applications have been presented from that the following of its advantages can be mentioned:

1. The conclusion in this model that anharmonicity is the result of phonon-phonon interaction leads to using the powerful quantum statistical method with annihilation and creation operators in derivation of the considered XAFS quantities.

2. The derived anharmonic interatomic effective potential can be considered as a new potential model which provides meaningful simplifications of the complicated many-body problem in materials studies: - Taking the many-body effects of the considered material into account by including the first shell near neighbor

contributions to the vibrations between absorber and backscatter atoms, - By projecting the first shell near neighbor contributions along the bond direction the one-dimensional model has been recovered.

3. By using the only Einstein frequency the calculations and analysis of the considered XAFS quantities in a quantum statistical problem have been reduced and simplified, yet provide the good agreement of the obtained results with the experimental data.

4. The description of XAFS quantities in terms of second cumulant leads to the advanced method based on which all the considered theoretical and experimental XAFS quantities including XAFS spectra and theier Fourier transform magnitudes, as well as those which are difficult to be directly measured have been obtained and extracted from the calculated and measured second cumulant or MSRD.

5. Based on the obtained temperature-dependent theoretical and experimental XAFS cumulants and thermal expansion coefficient the thermodynamic properties of the considered material have been in detail analyzed and valuated. They include the evident anharmonic effects and satisfy all their fundamental properties in temperature dependence, as well as approach the classical values at high-temperatures and contain zero-point energy contributions at low-temperatures, a quantum effect.

6. The XAFS spectra containing the obtained cumulants and their Fourier transform magnitudes provide the accurate structural determination of the considered material.

All the above results illustrate the simplicity and efficiency of the ACEM in XAFS data analysis and in materials studies.

Acknowledgements

The author thanks Prof. J. J. Rehr, Prof. Paolo Fornasini and Prof. R. R. Frahm for useful comments and cooperation.

REFERENCES

1. E. D. Crozier, J. J. Rehr, and R. Ingalls (1988), in *X-ray Absorption*, edited by D. C. Koningsberger and R. Prins (Wiley, New York). Chap. 9;

2. N. V. Hung, N. B. Duc, and R. R. Frahm (2003), *J. Phys. Soc. Jpn*. 72, 1254;

3. J. M. Tranquada and R. Ingalls (1983), *Phys. Rev*. B 28, 3520;

4. A. I. Frenkel and J. J. Rehr (1993), *Phys. Rev.* B 48, 585;

5. T. Miyanaga and T. Fujikawa (1994), *J. Phys. Soc. Jpn*. 63, 1036 and 3683;

6. N. V. Hung and J. J. Rehr (1997), Phys. Rev. B 56, 43;

7. R. P. Feynman (1972), *Statistical Mechanics*, Benjamin Reading;

8. E. A. Stern, P. Livins, and Zhe Zhang (1991), Phys. Rev. B 43, 8850;

9. L. A. Girifalco V. G. Weizer (1959), Phys. Rev. 114, 687;

10. S. a Beccara, G. Dalba, P. Fornasini, R. Grisenti, F. Pederiva, A. Sanson (2003), Phys. Rev. B 68, 140301(R);

11. R. B. Greegor and F. W. Lytle (1979), Phys. Rev. B 20, 4908;

12. T. Yokoyama, T. Susukawa, and T. Ohta (1989), Jpn. J. Appl. Phys. 28, 1905;

13. Y. S. Toukian, R. K. Kirby, R. E. Taylor, and P. D. Desai (1975), *Thermophysical Properties of Matter* (IFI/Plenum, New York);

14. N. V. Hung, T. S. Tien, N. B. Duc, and D. Q. Vuong (2014), *Mod. Phys. Lett.* B 28, 1450174;

15. N. V. Hung (2004), *Communications in Phys.* (CIP) Vol 14, No. 1, 7-14;

16. N. V. Hung, T. S. Tien, L. H. Hung, R. R. Frahm (2008), *Int. J. Mod. Phys*. B 22, 5155;

17. N. V. Hung, C. S. Thang, N. B. Duc, D. Q. Vuong, T. S. Tien (2017), *Phys.* B 521, 198-203;

18. J. J. Rehr, J. Mustre de Leon, S. I. Zabinsky, R. C. Albers, J. Am. Chem (1991), Soc. 113 5135;

19. W. Klysubun, P. Sombunchoo, W. Deenam, C. Komark (2012), *J. Synchrotron Rad*. 19, 930;

20. V. Pirog, T. I. Nedoseikina, A. I. Zarubin, A. T. Shuvaev (2002), *J. Phys.: Condens. Matter* 14, 1825;

21. I. V. Pirog and T. I. Nedoseikina (2003), *Physica* B 334, 123;

22. M. Daniel, D. M. Pease, N. Van Hung, J. I. Budnick (2004), *Phys. Rev*. B 69, 134414;

23. P. Fornasini and R. Grisenti (2015), *J. Synch. Rad.* 22, 1242-1257;

24. S. C. Gairola (2016), *Act. Phys. Polonica A* 129, 1141-1146.

Mô hình Einstein tương quan phi điều hòa và một số ứng dụng trong nghiên cứu các thuộc tính nhiệt động lực học và xác định cấu trúc của vật liệu

Nguyễn Văn Hùng[a*]

Thông tin bài viết

Ngày nhận bài:
19/4/2018
Ngày duyệt đăng:
12/6/2018

Từ khoá:
Hệ số Debye-Waller, khai triển cumulant, XAFS, các thuộc tính nhiệt động lực học.

Tóm tắt

Bài báo này trình bày mô hình Einstein tương quan phi điều hòa trong nghiên cứu các hệ số Debye-Waller dưới dạng khai triển cumulant và một vài ứng dụng của nó. Mô hình được dẫn giải dựa trên lý thuyết thống kê lượng tử. Ở đây, vấn đề phức tạp của hệ nhiều hạt đã được đơn giản hóa bằng việc diễn giải thế tương tác nguyên tử hiệu dụng phi điều hòa mà bao gồm các ảnh hưởng của hệ nhiều hạt với đóng góp của các dao động giữa các nguyên tử hấp thụ và tán xạ lân cận lớp thứ nhất và bằng cách chiếu những đóng góp này dọc theo hướng liên kết trong mô hình một chiều. Thế Morse được giả định để mô tả thế tương tác nguyên tử đơn cặp. Các kết quả tính toán số cho một số vật liệu phù hợp tốt với thực nghiệm chỉ ra sự phụ thuộc tất yếu vào nhiệt độ của các thuộc tính nhiệt động lực học, các hiệu ứng phi điều hòa và các tham số cấu trúc của vật liệu được xem xét.